Title

Detecting unitary synaptic events with machine learning.

Journal

Proceedings of the National Academy of Sciences, 121(6)

Authors

Wang, Nien-Shao

Marino, Marc

Malinow, Roberto

Publication Date

2024-02-06

DOI

10.1073/pnas.2315804121

Peer reviewed

PNAS RESEARCH ARTICLE | BIOPHYSICS AND COMPUTATIONAL BIOLOGY
NEUROSCIENCE

Detecting unitary synaptic events with machine learning

Nien-Shao Wang[a], Marc Marino[a], and Roberto Malinow[a,1]

Contributed by Roberto Malinow; received September 11, 2023; accepted December 14, 2023; reviewed by Bo Li and Simon Rumpel

Spontaneously occurring miniature excitatory postsynaptic currents (mEPSCs) are fundamental electrophysiological events produced by quantal vesicular transmitter release at synapses. Their analysis can provide important information regarding pre- and postsynaptic function. However, the small signal relative to recording noise requires expertise and considerable time for their identification. Furthermore, many mEPSCs smaller than ~8 pA are not well resolved (e.g., those produced at distant synapses or synapses with few receptor channels). Here, we describe an automated approach to detect mEPSCs using a machine learning–based tool. This method, which can be easily generalized to other one-dimensional signals, eliminates inter-observer bias, provides an estimate of its sensitivity and specificity and permits reliable detection of small (e.g., 5 pA) spontaneous unitary synaptic events.

synapse | miniature | machine learning

Significance

Spontaneously occurring quantal events produced by vesicular transmitter release at synapses generate an electrophysiological signal that can provide important information regarding pre- and postsynaptic function. The small signal relative to recording noise makes their identification by even well-trained individuals time-consuming and inconsistent across studies. Here, we describe an automated approach to detect small signals within noise using a machine learning-based tool. This method, easily generalized to other one-dimensional signals, eliminates inter-observer bias, provides a measure of its sensitivity and specificity, and permits reliable detection of small spontaneous synaptic events.

The first spontaneously occurring miniature excitatory postsynaptic signals were recorded at the neuromuscular junction (1). These events were subsequently shown to be due to the release of a single vesicle containing neurotransmitter and provided the basis for the quantal theory of synaptic transmission (2, 3). Since then miniature quantal events have been recorded in numerous preparations, and their properties (e.g., quantal size, quantal content and quantal event frequency) have been used to make conclusions regarding pre- and postsynaptic function (reviewed in ref. 4). For instance, the number or function of receptors is reflected in quantal amplitude; while the number of synapses or their probability of transmitter release correlates with quantal frequency. While there are notable exceptions to such correlations (e.g., refs. 5–7; reviewed in ref. 8), the amplitude and frequency of quantal events continue to be widely used as measures of synaptic function.

One important caveat to such use of miniature events is that many quantal events are small and cannot be distinguished from the recording noise. Because of this complication, signaling events that are smaller than the recording noise are generally not detected and thus not counted. An increase in receptor number or receptor function at synapses producing such events can render quantal events greater than the noise and thus detectable upon analysis. Such analyses can misattribute actual postsynaptic changes to be of presynaptic origin [e.g., during long-term potentiation (5–7)].

While some algorithms have been written to detect miniature events (9, 10) in practice many (and of greatest concern, an unknowable number of) small events are not detected. Furthermore, most algorithm-based detection is time-consuming and requires the eye of a well-trained scientist to confirm or reject detected events. A fast, sensitive, and accurate algorithm that detects and measures miniature events, which does not require human observation, and importantly provides an estimate of the sensitivity and specificity of detecting events of a given amplitude, would be of considerable benefit to the cellular neuroscience community.

Artificial neural networks (ANN), employed in machine learning, have recently been widely used to detect 1- and 2-dimensional patterns in a noisy background (11, 12). Given that miniature excitatory synaptic currents (mEPSCs) have a distinct shape that in general differs from noise, we examined how well a trained ANN could detect small mEPSCs embedded in electrophysiological recording noise.

Results

The use of an ANN requires two phases: training and testing.

ANN Training. To detect a signal within noise, the ANN was trained using an equal number of examples known to be signal or noise. Examples of noise were obtained from patch clamp electrophysiological recordings from a hippocampal neuron, wherein postsynaptic receptors were pharmacologically blocked or recording intervals were chosen that had no obvious signals. Each example consisted of 300 consecutive values from a recording interval

Author affiliations: [a]Center for Neural Circuits and Behavior, Division of Biology, Department of Neurosciences, University of California at San Diego, La Jolla, CA 92093

Author contributions: N.-S.W., M.M., and R.M. designed research; performed research; analyzed data; and wrote the paper.

Reviewers: B.L., Cold Spring Harbor Laboratory; and S.R., Johannes Gutenberg-University.

The authors declare no competing interest.

[1]To whom correspondence may be addressed. Email: rmalinow@ucsd.edu.

This article contains supporting information online at https://www.pnas.org/lookup/suppl/doi:10.1073/pnas.2315804121/-/DCSupplemental.

Published January 31, 2024.

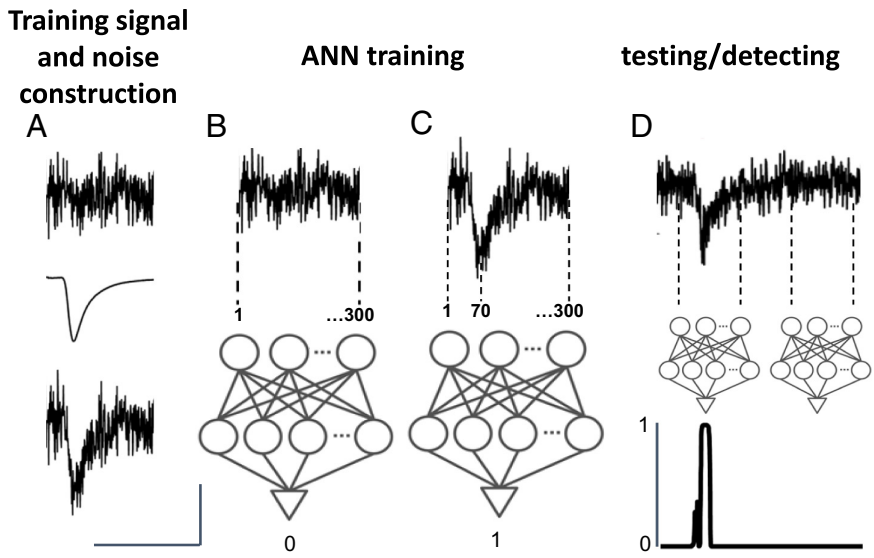

Fig. 1. ANN training and testing protocols. (*A*) *Top*, noise from electrophysiological recording; *Middle*, simulated mEPSC (*Materials and Methods*); *Bottom*, sum of *Top* and *Middle*. (Scale bars: 10 pA, 30 ms.) (*B* and *C*) Training of ANN with noise (*B*) and signal (*C*) examples. Locations 1 to 300 on training examples shown. *Bottom*, diagram of general ANN with output training values (0 and 1) indicated. See *Material and Methods* section for ANN details. (*D*) *Top*, two sections of recording noise + simulated mEPSC (not used during training) being tested with an ANN. Dashed lines indicate extent of tested sections. *Middle*, diagram ANN testing two different sections. *Bottom*, plot of CV trace resulting from application of the ANN to one-point moving windows. Y-axis: confidence value (0-1).

(e.g., 30 ms sampled at 10 KHz; Fig. 1 *A*, *Top*; see *Materials and Methods*). To generate examples of signal, we first produced an average of large, easily detected mEPSCs (Fig. 1 *A*, *Middle* and *SI Appendix*, Fig. S1). Examples of a signal consisted of the digital summation of examples of noise and the average mEPSCs scaled to different amplitudes and widths (Fig. 1 *A*, *Bottom*; see *Materials and Methods*). Importantly, the ANN was trained with mEPSC signals that peaked at a fixed location (in this case at location 70 of 300 pts; i.e., at 7 ms of a 30 ms trace; Fig. 1*C*). The neural net was trained to output a zero for noise and one for a signal peaking at location 70. Signal and noise examples used in ANN training and ANN testing were distinct.

ANN Testing. The output of a trained ANN for a test 300-point input was a single value; a confidence value (CV) continuously ranging from 0 to 1 indicating the confidence level the ANN ascribed the test input to be noise (i.e., values toward 0, Fig. 1*B*) or signal peaking at location 70 (i.e., values toward 1, Fig. 1*C*). A recording was tested by systematically applying the ANN to a sliding 300-point window of the recording trace, the window moving one point at a time (Fig. 1*D*). This procedure generates a CV trace of length the same as the recording trace (minus 300 pts). The CV output for a pure noise input is very close to 0; i.e., noise was well identified. Interestingly, as a mEPSC entered a 300-point window, the CV abruptly increased, with a CV peak that coincided quite well with the peak of a digitally placed mEPSC (Fig. 1*D*). We identified peaks in the CV trace using the Matlab findpeaks function (see ref. 13). We thus used the location of each CV peak as the potential location of a mEPSC in the recording.

Examples displaying the use of an ANN to detect mEPSCs in a section of a test recording, wherein synthetic mEPSCs were digitally added to recording noise at regular intervals, are shown in Fig. 2 (mEPSC of amplitudes 2 to 15 pA), Fig. 3 (mEPSC amplitudes between 3.5 to 4.5 pA), and *SI Appendix*, Fig. S2

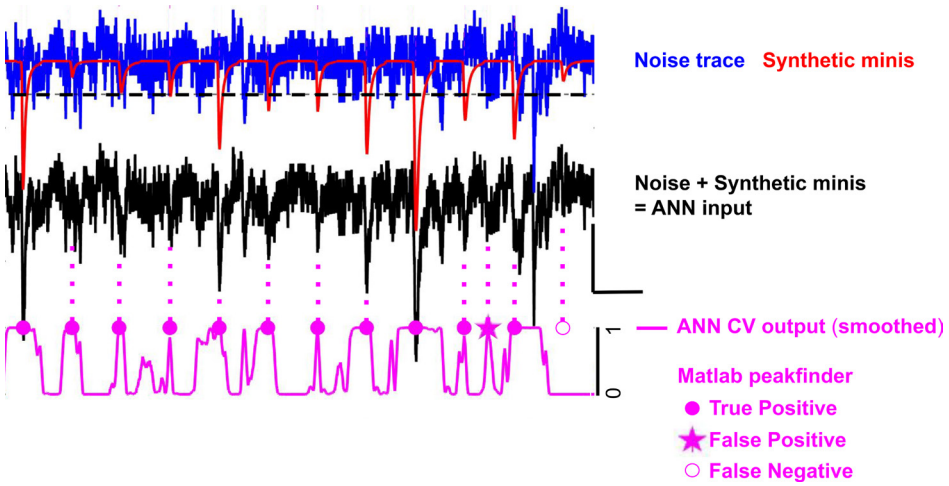

Fig. 2. ANN faithfully detects synthetic mEPSCs embedded in electrophysiological noise. Examples of noise from electrophysiological recording (blue), synthetic mEPSCs (3 to 15 pA; placed every 30 ms; red), their digital sum (black); sliding window of digital sum is input into ANN producing output CV trace (magenta). Matlab peakfinder function detects peaks on CV trace. True positive, false positive and false negative detection of mEPSCs indicated by filled circles, stars, and open circles respectively. Dashed vertical lines, location of detected mEPSCs (or undetected false negative mEPSC); horizontal dashed line indicates 5 pA. See *SI Appendix*, Fig. S7 showing that flat-appearing CV regions have small peaks accurately detected by Matlab peakfinder function. Scale bars: 10 pA; 30 ms.

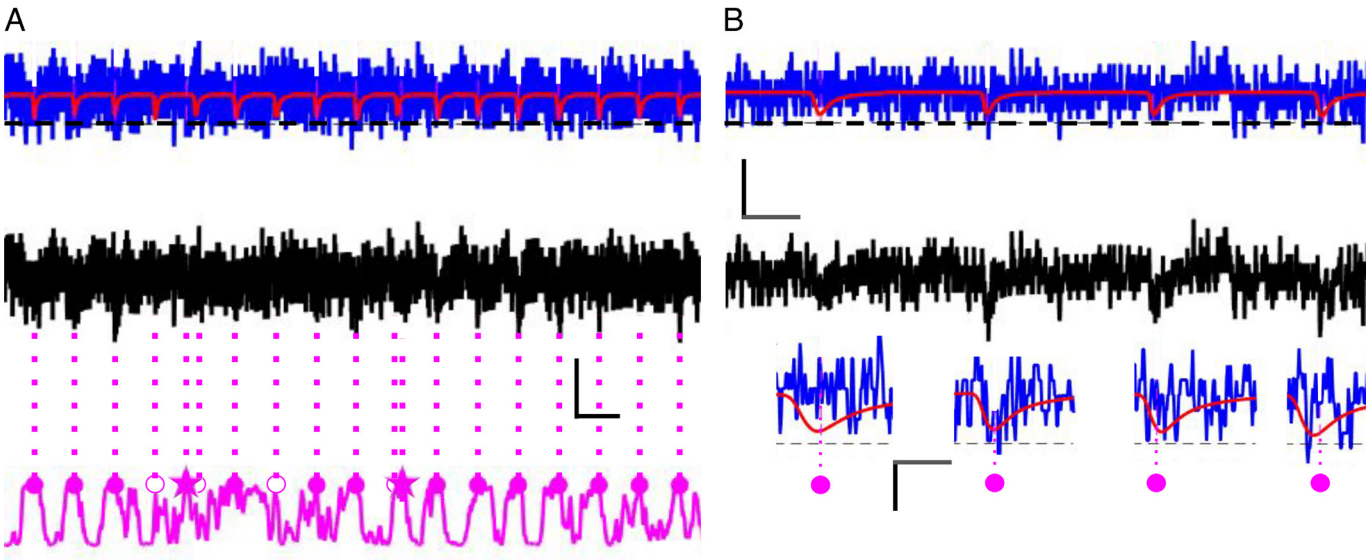

Fig. 3. ANN faithfully detects small synthetic mEPSCs (3.5 to 4.5 pA) embedded in electrophysiological noise. Same labeling as Fig. 2. (*A* and *B*) Low (*A*) and high (*B*) temporal resolution. Note accurate temporal detection of mEPSC peaks. (Scale bars, *A*, 10 pA, 30 ms; *B*, *Top*, 10 pA, 10 ms.) *Insets*: higher resolution of mEPSCs identified above. (*Inset* scale bars, 5 pA 3 ms.) Note, different noise used in Figs. 2 and 3.

(mEPSCs positioned at random times). Since the true position of synthetic mEPSCs was known, the true positive, false positive, and false negative events could be identified (indicated on Figs. 2 and 3). Note that many true positive mEPSCs detected by the ANN (particularly in Fig. 3) would be difficult for even a well-trained scientist to detect visually. Furthermore, the location of the peak of a detected mEPSC coincided well with the true location of the synthetic mEPSC (see Fig. 3*B*, insets; Fig. 5*C*).

This machine learning–based algorithm converts the problem of detecting mEPSCs in noise to a problem of detecting CV peaks that correspond to mEPSCs. Since the ratio of signal to noise (S/N) in the CV trace is typically much greater than the S/N in the electrophysiological recording (e.g., see Fig. 1*D*), we reasoned that detecting CV peaks could be achieved with greater accuracy. To measure the accuracy of an ANN in detecting mEPSCs, we used receiving operator characteristic (ROC) curves (14). We note that assigning peaks on a CV trace depends on setting a peak prominence threshold value as well as a CV trace smoothing window value. We used ROC curves (example shown in Fig. 4) to choose optimally these values (*Materials and Methods* and *SI Appendix*, Figs. S3 and S4). In ROC curves we plotted the true positive rate (TPr) versus the false detection rate (FDr; the fraction of detected events that were false) rather than false positive rate (FPr; the fraction of detected events that were divided by all possible detected locations; plots with FDr and FPr are compared, *SI Appendix*, Fig. S5). Since the number of all possible detected locations is the number of all sampled values in a trace and a very large number, the FPr is very small and not very informative. Meanwhile, the fraction of detected events that are false is more informative.

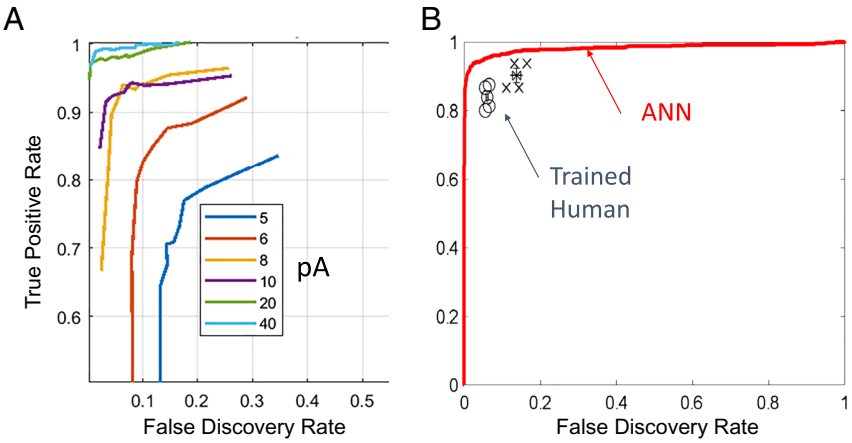

Fig. 4. ROC curves for ANN detection of mEPSCs and comparison to trained human observer. (*A*) ROC curves for detection of synthetic mEPSCs of different amplitudes (indicated by different colors) with ANN (*Materials and Methods*: *Generating ROC curves for a specific recording*). Recording noise for generating this ROC is displayed in Fig. 2. (*B*) ROC for ANN detection of synthetic mEPSCs (4 to 15 pA) embedded in noise trace (red line). Trained human observer was given same trace to analyze for mEPSCs, divided into four separate sections. True positives and false detections were counted for each of the four sections (open circles). Observer was subsequently told that several small mEPSCs were missed. Second observation (X symbols) produced more true positives and false detections. Note that in both observation periods, the human was outperformed by the ANN. Human required about 20 min to perform task. ANN task was performed in a few seconds.

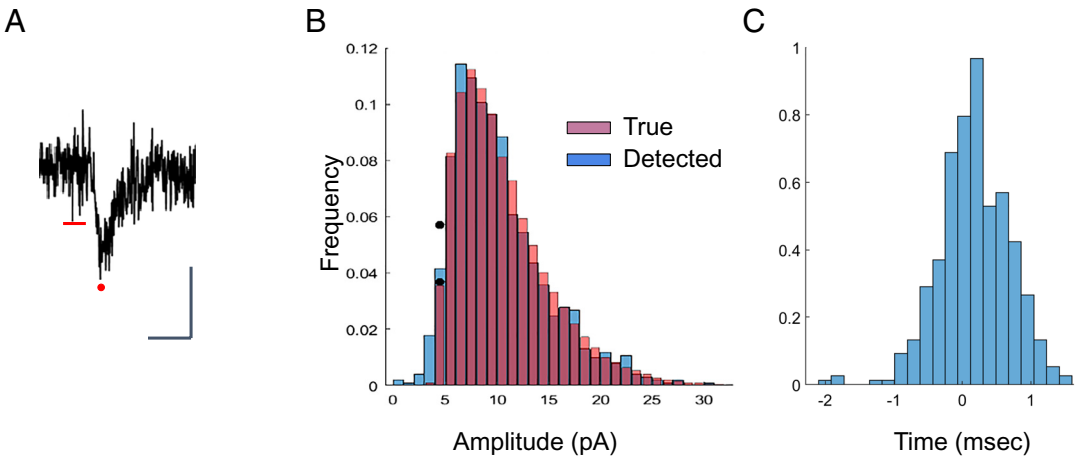

Fig. 5. Amplitudes of detected mEPSCs match well that of true mEPSCs. (*A*) example mEPSC with peak (red circle) and baseline period (red line) indicated. Amplitude is measured as the difference between mean of values 1 ms before and after detected peak (red filled circle) and mean of values in a 10 ms window ending 5 ms prior to the peak. (*B*) Frequency distribution histogram plotting the ground truth mEPSCs amplitudes (red bars) and amplitudes of mEPSCs detected by ANN (blue bars). Note that the number of mEPSCs of amplitude greater than 4 pA detected by ANN match well the true number of such mEPSCs. Black circles indicate upper and lower estimates of detected mEPSC between 4 and 5 pA provided by scaling detected mEPSC frequency with 1/TPr (upper estimate) and 1-FDr (lower estimate). (*C*) Frequency distribution histogram plotting the difference between detected mEPSC time and ground truth time for detection of 20 pA mEPSC.

Comparison of ANN to Human. A human observer was given a noisy trace (~10 min recording; 10 KHz sampling; divided into four sections) containing synthetic mEPSCs (approximately 4 to 15 pA; e.g., Fig. 5*B*, true events) to analyze; TPr and FDr were computed. The observer was subsequently told that they had missed several small mEPSCs; upon re-examination, more true positive and false detection were counted (See Fig. 4*B*, symbols). The same trace was analyzed by an ANN, and an ROC curve was calculated (See Fig. 4*B*, red line). mEPSC detection by ANN was more accurate and faster (human required ~20 min; ANN required a few seconds) than that of a trained human.

Computing mEPSC Amplitude. To compute the amplitude of a detected mEPSC, we subtracted the peak value (mean of values 1 ms before and after the detected mEPSC peak location) from a baseline value (mean of values at 5 to 10 ms prior to the detected location; See Fig. 5*A*). Digitally generated mEPSCs placed on a noisy background (noise standard deviation = 2.6 pA) were detected and their amplitude was measured. Comparison of the amplitude distribution of detected mEPSCs with true amplitude distribution shows a good match (Fig. 5*B*). Approximately 30% of true mEPSCs ranged between 5 and 8 pA, most of which were accurately detected. In many recordings, such mEPSCs would be missed by humans using current mEPSCs detection algorithms. Note that the location of detected mEPSCs is also quite accurate (Fig. 5*C*).

Discussion

Measuring miniature synaptic events is a widely used electrophysiological technique to make conclusions regarding pre- or postsynaptic function. Here, we provide a simple method based on machine learning that can detect very small events. The specificity and sensitivity of the method, measured using ROC curves, can be readily computed, providing confidence for which mEPSCs are being accurately detected. Future studies should investigate the dependence of the method on several variables (listed in *Materials and Methods* section) for which we made a choice based on experience with the method. Signals that occur very frequently (>~50 Hz), which will degrade the appearance of the signal (e.g., mEPSC), will be difficult to resolve with this method. Simulations on electrical models of neurons may provide estimates regarding the fewest number of open synaptic receptors that may be expected to be detected.

It should be noted that there are potentially many electrophysiological signals (e.g., miniature inhibitory currents; in vivo recorded extracellular action potentials; etc.) or signals with expected shapes in other one-dimensional data, which could be analyzed in a similar manner. Given that spontaneous events are more difficult to detect, similar methods applied to time-locked events (e.g. evoked EPSCs) should provide even better results.

Note: during the preparation of this manuscript, which was initially published as a PhD thesis (15), a new study was published using unsupervised machine learning (16), rather than supervised learning used in this study.

Materials and Methods

All computations were performed using Matlab, although the method described in this study could be carried out using other platforms (e.g., Python, …) that can employ machine learning tools. The trained human observer referred to above provided consent to analyze test data.

Generating an ANN. Standard machine learning methods were used to generate an ANN (12, 13). In brief, a feedforward neural network was used with architecture consisting of one input layer, three hidden layers, followed by an output layer. The input layer had a size of 300, one for each time point of the signal. The three hidden layers had sizes 200, 100, and 100 respectively, each applying a sigmoid activation function. As is the standard for most classification tasks, softmax function was used as the activation function for the output layer which provided the probability distribution of the two classes: signal and noise. For training, the loss function of the model was defined as the cross entropy between the two target labels. To minimize the loss function, scaled conjugate gradient backpropagation method was used with sigma and lambda set to 5e-05 and 5e-07 respectively.

Then, 1,000 samples of signals and noise each were used for ANN training. For signals, two sets of mEPSCs were used, each set was generated by varying the amplitude and width of a fast and slow mEPSC (*SI Appendix*, Fig. S1). The mEPSC amplitude was set by the equation:

$$\text{mEPSC amplitude} = 3 + K * (\text{pearsrnd}(10, 3, .5, 3, 1, 1)\text{^}2) / 100 \text{ pA},$$

where K = 1.5* noise SD, pearsrnd = random numbers drawn from the distribution in the Pearson system with values pearsrnd (mean, sigma, skew, kurt, returned matrix columns, returned matrix rows).

mEPSC widths were set by the equation:

$$\text{mEPSC width} = (\text{width at half peak maximum of mEPSC in Fig. 1}) * 1/(0.6 + .4 * \text{rand}(0, 1)).$$

Generating ROC Curves for a Specific Recording. To generate an ROC curve, the ANN is applied to a noisy trace (see below) containing 1,000 digitally added mEPSCs of widths as described above and of amplitude **a** pA (typically one of 10 integer values between 3 and 20 for each curve, see Fig. 3) placed at a set of known locations, (e.g., every 60 ms apart) indicated by the set {**TrueLocations**}. The set of locations detected by the MATLAB "peakfinder" function on the **N**-point smoothed CV trace with "peakfinder prominence" set at **T** is indicated by the set $\{\textbf{DetectedLocations}\}_{NT}$. The set $\{\textbf{DetectedLocations}\}_{NT}$ can be compared with {**TrueLocations**}. If a location in $\{\textbf{DetectedLocations}\}_{NT}$ is within 2 ms of a location in {**TrueLocations**}, the detected location is considered a true positive. If a location in $\{\textbf{DetectedLocations}\}_{NT}$ is not within 2 ms of a location in {**TrueLocations**}, the detected location is considered a false positive. To improve detection of mEPSCs occurring within short time periods (e.g., ~20 ms), a CV trace can be analyzed several times, removing a detected mEPSC (from peak location −50 to +150 locations – −5 to +15 ms if sampling is 10 KHz) from a trace once identified. As only the first of nearby mEPSCs is generally identified, subsequent analysis will identify more mEPSCs. Thus, for each set of **N** and **T** values, a TPr (the number of true positives detected divided by the number of digitally placed true positives) and a FDr (the fraction of events detected that were not true positives) is generated, producing a point on an ROC curve. By changing **T**, different points on the ROC curve are produced (e.g., reducing **T** increases the TPr at the expense of a larger FDr; see *SI Appendix*, Fig. S3*A*). In detecting a specific amplitude mEPSC, different ROC curves for different smoothing values are shown in *SI Appendix*, Fig. S3*B*.

We wished to display all ROC curve values (for different values of **T** and **N**) on a single diagram. For this purpose, for each point on an ROC curve, we computed a "distance to perfect detection" (**Dtpd**); that is, the distance of an ROC point to the upper left corner, the location with 100% TPr and 0% FDr (*SI Appendix*, Fig. S2). For instance, at a point on the ROC curve with 0.85 TPr and 0.1 FDr, the **Dtpd** value is $((0.1^2 + (1 - 0.85)^2)^{0.5} = 0.18$. For easier viewing, we computed −log10(**Dtpd**) values for different **N** and **T** values for detection of a specific amplitude mEPSC and displayed this as a heatmap (*SI Appendix*, Fig. S3*C*). Warm colors correspond to higher −log10(**Dtpd**) values; that is, CV smoothing and threshold values that produce an ROC value closest to perfect mEPSC detection. In this case, for an ANN detecting a 3 pA mEPSC, the optimal CV threshold (0.975) and CV smoothing (5 point average) values produced a −log10(**Dtpd**) = 1.15; or **Dtpd** = .07, meaning that for these CV **T** and **N** values, the TPr was ~0.95 and FDr was ~0.05. We note that values in these heatmaps, which correspond to the accuracy of an ANN, could differ by ~10 to 20% for different ANNs generated from the same recording. We thus generated >10 trained networks and chose the one with the best detection (as indicated by peak value in a heat map).

Heat maps such as these were generated for ROC curves corresponding to detection of different mEPSC amplitudes (*SI Appendix*, Fig. S4). Note that the optimal **N** and **T** values (warmest location on a heat map) differed slightly for detection of different amplitude mEPSCs. **N** and **T** for analysis of mEPSCs of variable amplitude values are based on an average of heatmaps obtained for 5, 6, 8, 10, and 20 pA.

Confidence limits in detection of a specific amplitude range can be computed from TPr and FDr in an ROC curve. The detected frequency in an amplitude distribution histogram is scaled by 1/TPr to estimate the upper bound and 1-FDr to estimate the lower bound.

Identification of Peaks on CV Trace. The smoothed CV trace was analyzed using the peakfinder MATLAB function, using the following variables: MinPeakDistance = 1 pt; MinPeakProminence = **T**; MinPeakWidth = 1 pt. The values for the smoothing window and **T** were chosen based on the optimal smoothing window and threshold value observed from the mean heat map described above. If detected locations were within 2 ms of true locations, they were deemed true positives. Otherwise, they were deemed false positive locations.

Measuring mEPSC Amplitude. See Fig. 5. Amplitude of mEPSC identified on recording trace is measured by first identifying mEPSC peak: the minimum value on recording within 2 ms of location identified by CV trace (as above). mEPSC peak value (MPV) is obtained by averaging values on the recorded trace from 1 ms before to 1 ms after the mEPSC peak location. mEPSC peak baseline (MPB) is obtained by averaging values from 10 ms before to 5 ms before mEPSC peak location. mEPSC amplitude = MPV − MPB. Note that accurate detection of a mEPSC origin can be determined by using the method described in this study, by choosing the origin of a simulated mEPSC as the reference point (rather than the mEPSC peak).

Detection of mEPSC with Different Levels of Noise. As the noise in the recording increases, it is expected that the detection accuracy will be reduced. This is shown (*SI Appendix*, Fig. S6) for the detection of mEPSCs with amplitude 6 pA and the background standard deviation of the noise varied from 2 to 4 pA.

Hyper Features. The impact of the values of some variables used in the algorithm discussed in this study were examined only to a limited degree. These include, but are not limited to, the variables listed below. A more robust determination of optimal values is likely warranted. Signal-to-noise ratio of training samples, perhaps related to the noise of analyzed file; number of training samples; Matlab findpeaks variables "MinPeakDistance," "MinPeakWidth"; in ROC generation, random location specifications, time window to accept as accurate detection, and time window used for mEPSC removal in repeatedly analyzed traces.

Data, Materials, and Software Availability. Code data have been deposited in github (17) (to be provided in future). All other data are included in the manuscript and/or *SI Appendix*.

ACKNOWLEDGMENTS. We thank the reviewers and Jeff Isaacson for critical reading of an earlier version of this manuscript. We thank Helmut Kessels for providing raw noise samples used in this study.

1. P. Fatt, B. Katz, Spontaneous subthreshold activity at motor nerve endings. *J. Physiol.* **117**, 109–128 (1952).
2. J. del Castillo, B. Katz, Quantal components of the end-plate potential. *J. Physiol.* **124**, 560–573 (1954).
3. G. Palade, Electron microscope observations of interneuronal and neuromuscular synapses. *Anat. Rec.* **118**, 335–336 (1954).
4. A. R. Martin, Quantal nature of synaptic transmission. *Physiol. Rev.* **46**, 51–66 (1966).
5. J. T. Isaac, R. A. Nicoll, R. C. Malenka, Evidence for silent synapses: Implications for the expression of LTP. *Neuron* **15**, 427–434 (1995).
6. D. M. Kullmann, Amplitude fluctuations of dual-component EPSCs in hippocampal pyramidal cells: Implications for long-term potentiation. *Neuron* **12**, 1111–1120 (1994).
7. D. Liao, N. A. Hessler, R. Malinow, Activation of postsynaptically silent synapses during pairing-induced LTP in CA1 region of hippocampal slice. *Nature* **375**, 400–404 (1995).
8. H. L. Atwood, J. M. Wojtowicz, Silent synapses in neural plasticity: Current evidence. *Learn. Mem.* **6**, 542–571 (1999).
9. A. J. Pernía-Andrade *et al.*, A deconvolution-based method with high sensitivity and temporal resolution for detection of spontaneous synaptic currents in vitro and in vivo. *Biophys. J.* **103**, 1429–1439 (2012).
10. Y. G. Kim, J. J. Shin, S. J. Kim, Minhee analysis package: An integrated software package for detection and management of spontaneous synaptic events. *Mol. Brain* **14**, 138 (2021).
11. S. Dreiseitl, L. Ohno-Machado, Logistic regression and artificial neural network classification models: A methodology review. *J. Biomed. Inform.* **35**, 352–359 (2002).
12. Y. LeCun, Y. Bengio, G. Hinton, Deep learning. *Nature* **521**, 436–444 (2015).
13. H. B. Demuth, M. H. Beale, *MATLAB Neural Network Toolbox: User's Guide* (MathWorks, Inc, 1992).
14. F. S. Nahm, Receiver operating characteristic curve: Overview and practical use for clinicians. Korean J. Anesthesiol. **75**, 25–36 (2022).
15. M. J. Marino, "Generation of an artificial neural network to detect small signals in noisy electrophysiological data." PhD thesis, University of California San Diego, San Diego, CA (2020).
16. T. Pircher, B. Pircher, A. Feigenspan, A novel machine learning-based approach for the detection and analysis of spontaneous synaptic currents. *PLoS One* **17**, e0273501 (2022).
17. N.S. Wang, M.J. Marino, R. Malinow, Mini_Scripts. GitHub. https://github.com/mrreganwang/Mini_Scripts. Deposited 12 September 2023.